RSC Advances

PAPER

View Article Online
View Journal | View Issue

Cite this: RSC Adv., 2014, 4, 34168

Polyaniline nanofibers–graphene oxide nanoplatelets composite thin film electrodes for electrochemical capacitors†

Mohd. Khalid,*[a] Milton A. Tumelero,[a] Vinicius C. Zoldan,[a] Cristiani C. Pla Cid,[a] Dante F. Franceschini,[b] Ronaldo A. Timm,[c] Lauro T. Kubota,[c] Stanislav A. Moshkalev[d] and Andre A. Pasa*[a]

Composite thin films of polyaniline (PANI) nanofibers and graphene oxide (GO) nanoplatelets are synthesized through a simple electrodeposition process for electrochemical capacitors. The morphology and structure of the materials are investigated by field emission scanning electron microscopy, transmission electron microscopy, current sensing atomic force microscopy, X-ray photoelectron spectroscopy, Fourier transforms infrared spectroscopy, X-ray diffraction, and ultraviolet-visible spectroscopy. In the process of electrodeposition, the electrostatic interactions between the oxygen-functionalized graphene and aniline monomers at an electrolyte interface assisted the co-deposition of PANI nanofibers and GO nanoplatelets. These thin films have an excellent effect on the electrochemical properties with an electrochemical capacitance of 662 F g^{-1} at a low current density of 0.025 mA cm^{-2} with simultaneous high energy density (64.5 W h kg^{-1}) and high power density (1159 W kg^{-1}). The excellent electrochemical performance of the films is attributed to the unique structure of the material, showing synergy between PANI nanofibers and GO nanoplatelets.

Received 17th April 2014
Accepted 15th July 2014

DOI: 10.1039/c4ra06145d

www.rsc.org/advances

1. Introduction

The development of alternative energy resources with elevated energy and high power density has received noteworthy attention since the end of the last century due to the depletion of fossil fuels and global warming.[1–3] Thin film electrochemical capacitors are the most promising energy sources known that can meet these demands. Electrochemical capacitors, also known as supercapacitors, provide higher power density than batteries and higher energy density than conventional capacitors. Despite these advantages, supercapacitors have lower energy density than batteries, and an enhancement in the energy density remains a significant challenge in supercapacitor research. Currently, much research on electrochemical capacitors has sought to achieve high specific capacitance with simultaneously high energy and high power densities at low production costs.[4,5] Based on the charge-storage mechanism, electrochemical devices could be divided into electrochemical double-layer capacitors and pseudocapacitors, in which energies are stored in the form of electrical double layers at the interface of the electrode/electrolyte and reversible redox reactions of the electroactive species, respectively. Conductive carbon-based materials are generally adopted as electrode materials for storing the charge through electrochemical double layers and can exhibit high power densities because of faster ion flow than that in redox reactions. On the other hand, conducting polymers and metal oxides are generally used as pseudocapacitor electrode materials, which store energy through electrochemical reactions and can exhibit high energy densities.

The synthesis and design of conducting polymers with carbon materials are important for the development of nanocomposite thin films, which can enable large-area, low-cost electrode material to be constructed. Among the conducting polymers, PANI is regarded as one of the most promising materials due to its excellent conductivity, high electrochemical activity, stability in air and water, low cost, and ease of synthesis,[6] although the application of PANI as supercapacitor material is rather limited due to its poor processing performance and cyclic stability. Therefore, it is often hybridized with carbon materials to prepare a composite and used in supercapacitors with better specific capacitance and mechanical stability.[7–10] Recently, graphene oxide has attracted substantial interest as a promising precursor for preparing graphene-based

[a]Laboratório de Filmes Finos e Superfícies, Departamento de Fisica, Universidade Federal de Santa Catarina, 88040-900-Florianopolis, Brazil. E-mail: mkansarister@gmail.com; andre.pasa@ufsc.br; Tel: +55 4884061547

[b]Instituto de Física, Universidade Federal Fluminense, Niterói-RJ, Brazil

[c]Departamento Química Analítica, IQ-UNICAMP, Campinas, SP, Brazil

[d]Center for Semiconductor Components, State University of Campinas, Campinas, SP, Brazil

† Electronic supplementary information (ESI) available. See DOI: 10.1039/c4rta06145d

composite materials. GO is the oxidized form of graphene, and its structure can be visualized as a graphene sheet with its basal plane and edges decorated by oxygen-containing groups.[11–13] It has been demonstrated that the presence of oxygen-containing functional groups on graphene facilitate the surface modification for making composites with conducting polymers. Recently, researchers have reported the synergistic combination of GO with conjugated polymers and their dramatic improvements in electrochemical properties.[14–18] Interestingly, GO has shown the excellent capacitance and good cycle durability than that of graphene.[19,20] Numerical methods have been explored to design new structure materials for PANI and graphene, most of the literature follows the simple solution mixing, *in situ* polymerization, and electropolymerization of aniline in the presence of GO or reduced GO.[21–28] Xu *et al.*[29] have demonstrated the hierarchical composites of polyaniline nanowire arrays on graphene oxides through a chemical method, which shows a high specific capacitance of 555 F g^{-1} at a discharge current density of 0.2 A g^{-1}. The composites of PANI and GO sheets for the purpose of supercapacitor development was recently reported by Zhang *et al.*,[30] which were synthesized *via* electrochemical method with high specific capacitance of 1136.4 F g^{-1} with a GO concentration of 10 mg L^{-1} at a scan rate of 1 mV s^{-1}. Feng *et al.*[31] showed PANI–graphene composites synthesized by an electrochemical reduction process with a high specific capacitance of 640 F g^{-1}, and another composite synthesized by the electropolymerization of PANI on the graphene electrode showing electrochemical capacitance of 223 F g^{-1}.[32] A PANI–graphene nanosheet composite with the specific capacitance of 1046 F g^{-1} was synthesized using *in situ* polymerization.[33]

In most of the work, PANI is either to be coated on graphene sheets or be covalently grafted on graphene sheets. However, very little attention has been paid to the electrochemical co-deposition of PANI and GO together. This work describes the co-deposition of PANI nanofibers and GO nanoplatelets in the form of thin films by using a one-step electrochemical polymerization method. The as-prepared PANI–GO films display remarkably enhanced electrochemical properties, compared with the pure PANI thin film. The excellent electrochemical performance (supercapacitance, high power and high energy densities) of PANI–GO films makes them promising electrode materials for electrochemical energy storage devices, such as thin film microbatteries and ultracapacitors.

2. Experimental section

2.1 Preparation of GO

GO was synthesized by a modified Hummers method.[34–36] Briefly, 2 g of graphite flakes (Nacional do Grafite; Graflake 99580; 99.50% purity) were dispersed in 98% (w/w) sulfuric acid at room temperature with a mechanical stirrer. After stirring for 15 min, 2 g of $KMnO_4$ (Sigma-Aldrich) were slowly added to the suspension, which acquired a green color due to the formation of the oxidizing agent (MnO_3^+). During this phase, the temperature was kept under 30 °C by using an ice bath. Additionally, two portions of $KMnO_4$ were added in a daily basis. The end of the oxidation was determined by the disappearance of the green color after adding the third portion of $KMnO_4$. At the end of the oxidation, the reaction mixture became very viscous due to the exfoliation of the formed GO layers. GO prepared by this described procedure was separated from the rest of the reaction mixture and purified. First, a few drops of 30% (w/w) H_2O_2 were added until the purple color disappeared. The resulting mixture was then centrifuged (Centribio, model 80-2B) at 1800*g* until the supernatant became clear. The supernatant was removed, and the precipitate was redispersed using an ice–water mixture, followed by an additional centrifugation at 1800*g*. This cycle was repeated twice using water, three more times with 5% (v/v) HCl and finally washing twice with distilled water again. The time spent in the centrifugation until the supernatant became clear increased after each cycle. The resulting dispersion of GO in water (3.3 mg mL^{-1}, pH ~ 5.0) was stored at ambient conditions.

2.2 Electrodeposition of PANI–GO composite films

Aniline was obtained from Sigma-Aldrich and distilled under vacuum to remove oxidation impurities before use. The electrodeposition of PANI–GO and PANI films was carried out in a one-compartment, three-electrode connected cell using a potentiostat (Autolab PGSTAT302N) electrochemical workstation at room temperature under computer control. The working and counter electrodes were indium–tin oxide (ITO)-coated glass slides (Lumtec Corp. 15 Ω) with surface areas of 4 cm^2 and a platinum sheet with a surface area of 4 cm^2, respectively. ITO glass slides were carefully cleaned by successive rinsing in a mixture of ethanol–acetone (1 : 1) and deionized water then dried under a gentle stream of nitrogen in sequence before use. The space between both electrodes was ~3 cm, and a saturated calomel electrode (SCE) was used as a reference electrode. In order to deposit PANI–GO on the ITO substrate, an electrolyte solution of 1 mol L^{-1} H_2SO_4 + 0.12 mol L^{-1} aniline with varying the contents of GO suspension from 0.05 to 0.2 mL was prepared in the following manner. A controlled volume of aqueous colloidal suspension of GO (3.3 mg mL^{-1}) was added in 100 mL of 1 mol L^{-1} H_2SO_4 and ultrasonicated for 1 h (dispersion was negligibly effect by ultrasonication); in the sequence, purified aniline monomer was added to this mixture and allowed to stir for 2 h at room temperature.

The electrolyte solutions were purged with nitrogen for 10 min before performing electrodeposition. For comparison, a pure PANI film was electrochemically synthesized in the absence of GO *via* a similar previous procedure. The all-electrochemical deposition processes were carried out at a constant applied oxidative potential of 750 mV *vs.* SCE. The electrodeposited films were rinsed gently with double-distilled water, dried under flowing nitrogen until a shiny green film had been obtained and stored in vacuum desiccators for several hours. Thus, the obtained PANI–GO films were labeled as PG-A, PG-B, and PG-C, for 0.05, 0.1, and 0.2 mL based on the feed amount of GO to the electrolyte solution, respectively. To investigate the mass of the deposited material, a QCM200 Quartz Crystal Microbalance was used. The thickness of the

films was measured by using Profilometer (Bruker). All solutions were prepared using Milli-Q grade water (18.2 MΩ cm).

2.3 General characterization

The morphologies of the materials were investigated with a JEOL JSM-6701F field-emission scanning electron microscope (FE-SEM) and JEOL JSM-2100 transmission electron microscope (TEM). For FE-SEM analysis, the electrodeposited film on the ITO was mounted on aluminum stubs and sputter-coated with gold. For TEM analysis, a small portion of the film was removed from the ITO surface with the help of a spatula, sonicated in ethanol, and a drop of solution was then dropped on copper microgrid. Infrared spectra (FTIR) were taken using a Perkin-Elmer Tensor 100 spectrometer in the range of 400–4000 cm^{-1}, and pellets were made from scratched material from the ITO substrate and mixed with KBr. X-ray diffraction (XRD) patterns of the samples were recorded with CuK_α radiation at the scan rate of 2° (2θ) min^{-1}. UV-visible (UV-vis) spectra of the samples were recorded from 200 to 1000 nm using a Perkin Elmer 750 spectrophotometer. XPS (X-ray photoelectron spectroscopy) were collected using a Phi Quantum 2000 (Physical Electronics) instrument with monochromatized Al Kα as the radiation source.

2.4 Current sensing AFM characterization

Current sensing-atomic force microscopy (CS-AFM) measurements were performed in air using a Pico-SPM (Molecular Imaging Corporation, USA) AFM operating in contact mode. Pt/Ir coating tips with a nominal force constant of 0.2 N m^{-1} and a tip curvature radius of 20 nm were used for the simultaneous imaging of topography and mapping of local changes of electrical conductance of the sample surface. Samples for the CS-AFM studies were mounted *via* silver paste to the AFM sample holder. *I–V* curves using the CS-AFM system on different points on the film surface were also performed to obtain the local character of electrical conductance. The *I–V* curves are the average of at least 20 measurements, and the image treatment and analysis were carried out using WSxM 4.0 Develop 12.1 software.

2.5 Electrochemical characterization

To evaluate the electrochemical experiments, the device was connected to an electrochemical workstation using alligator clips. The electrochemical behavior of the PANI–GO films was evaluated using cyclic voltammetry (CV), galvanostatic charge–discharge measurements, and electrical impedance spectroscopy (EIS). All electrochemical experiments were carried out in 1 mol L^{-1} H_2SO_4. The EIS analysis of the sample was done by superimposing a sinusoid perturbation of 5 mV over a zero-applied voltage and measuring the in- and out-phase current components for frequencies ranging from 10 mHz to 100 kHz. Two consecutive experiments were performed for each sample, whereas the first experiment was discarded to avoid charging effects. The equipment employed was a FRA2 model in an Autolab potentiostat. All electrochemical tests were carried out in a three-electrode cell, in which the counter electrode was a platinum foil, the working electrode was an electrodeposited film, and an SCE was used as the reference electrode.

3. Results and discussion

The current *vs.* time (*I–t*) curves were recorded during the electrochemical deposition of PANI–GO films and pure PANI film at a constant applied oxidative potential of 750 mV, as shown in Fig. 1. All *I–t* curves follow the same trend with current gradually increasing until reaching a saturation level.[37] In the electrolyte, the presence of protonic acid H_2SO_4 provides the necessary counter ions where the imine nitrogens of PANI are protonated. A wide range of oxygen functionalities (–OH, C–O–C, –COOH) bonded onto the surface of GO electrostatically interact with the aniline monomer and makes the complex in an aqueous electrolyte solution. As the electropolymerization of aniline is performed, the deposited PANI films contain both an acidic counter ion and GO onto the electrode surface. The incorporation of acidic counter ion in the PANI–GO film was verified by XPS analysis.

It is also expected that the oxygen functionalities of GO act as the charge compensating sites, which interact with the radical cations of the NH groups of the emeraldine salt form of PANI. The electrochemical properties of the PANI–GO films were compared with pure PANI film having only an acidic counter ion. The electrochemical setup and the digital images of electrodeposited films, as well as the possible interactions between aniline–GO and PANI–GO, are illustrated in Fig. 2. All samples that were further investigated in this work had thin solid films with thicknesses of about 148 ± 5 nm. The weight of the deposited material was recorded using a QCM. Considering the electrodeposited charge as a function of time and the thicknesses of the layers at different deposition times, it was possible

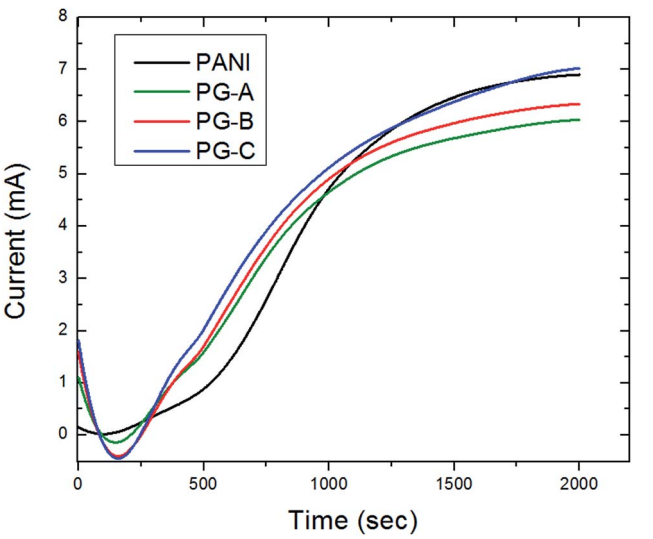

Fig. 1 Current *vs.* time transients recorded during electrodeposition at a constant oxidative potential of 750 mV. The electrolyte mixture was 0.12 mol L^{-1} aniline in 100 mL aqueous solutions of 1 mol L^{-1} H_2SO_4 + 0.05, 0.1, and 0.2 mL of GO colloidal suspension.

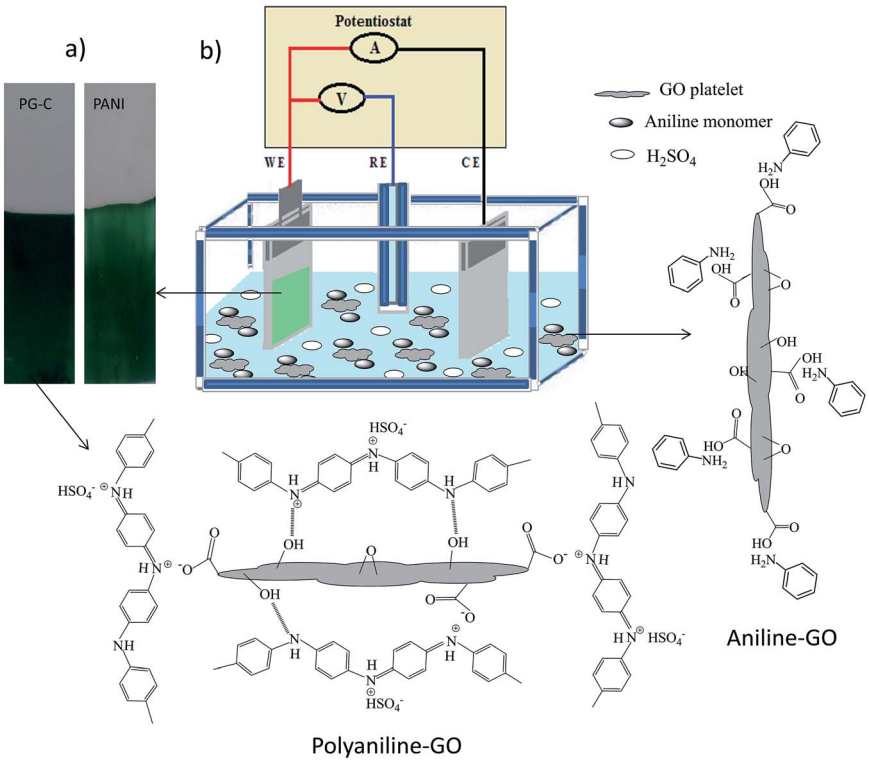

Fig. 2 (a) Representative digital photographs of pure PANI and PANI–GO thin films on ITO-coated glass slides and (b) experimental setup of electrochemical deposition and illustration of multiple possible interactions between aniline–GO and PANI–GO.

to calculate the mass density for the PANI sample with and without GO using the equation.

$$\rho = \frac{M\alpha}{QA}, \quad (1)$$

where ρ is the mass density, M is the electroplated mass, Q is the electrodeposited charge, A is the delimited area, and α is proportionality constant between the charge and thickness in C cm^{-1}. Fig. 3 displays the calculated mass density of each film for the different amounts of GO in the electrolyte. Because all samples present the same behavior, a rapid increase of density in the initial stages of electrodeposition, this effect can be attributed to a high compact growth of PANI nanofibers. Nevertheless, after dozens of nanometers in thickness, mass density starts to fall gradually, indicating the nucleation of fibers and other non-compact structures. Visible differences between the PANI–GO deposit samples can be seen; *i.e.*, by raising the amount of GO in the electrolyte, films become heavier. The linear relation between thin film mass and GO amount in the electrolyte is shown in the inset of the figure indicating that the mass of the films increased with increasing the amount of GO in the electrolyte. The mass of deposited materials were 60, 68, 82, and 120 μg for pure PANI, PG-A, PG-B, and PG-C samples, respectively.

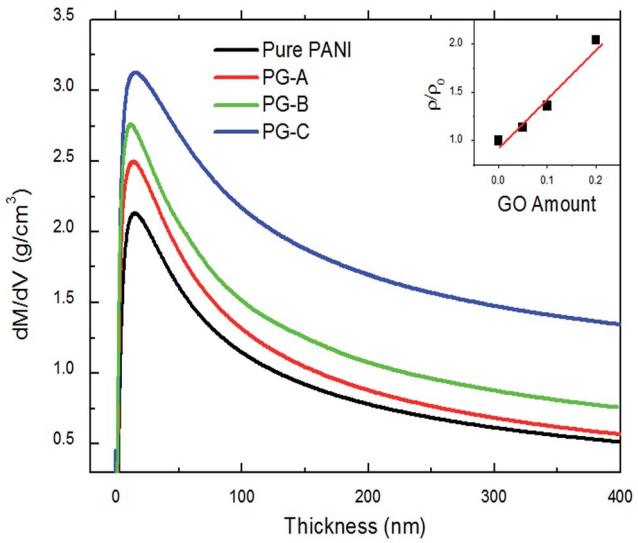

Fig. 3 Calculated mass density *vs.* thickness and inset shows the relative mass density *vs.* GO amounts, where ρ_0 = mass density of pure PANI and the curve obtained at 150 nm thickness of the films.

3.1 Morphological and structural characterization

The typical micromorphology of the resulting films was observed by FE-SEM and TEM. The FE-SEM micrographs of pure PANI and PANI–GO films as presented in Fig. 4 show the microstructure of the PANI nanofibers with and without GO. Random and highly interconnected network fibrillar morphology was observed for all samples. It could be seen that for all PANI–GO samples, the PANI nanofibers accompanied GO platelets as large as 1 μm. TEM imaging was used to determine the detailed nanoscale structure of PANI–GO films, as can be

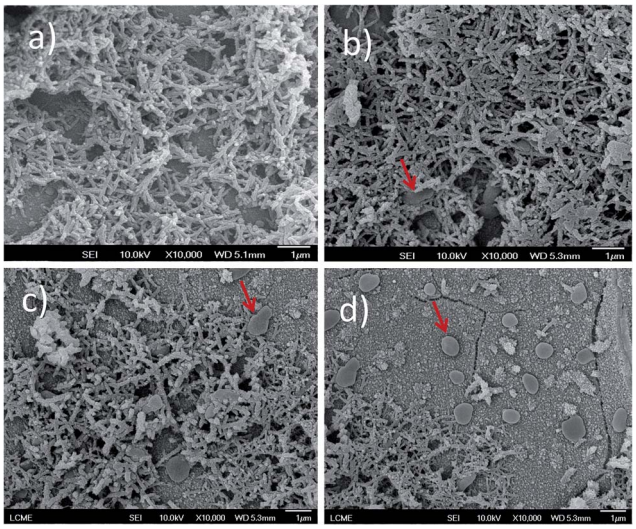

Fig. 4 SEM images of an interconnected network of nanofibers of (a) pure PANI, and (b–d) PAN–GO samples (PG-A, PG-B and PG-C), in which the red arrows point to the some large-size platelets of GO embedded with PANI nanofibers.

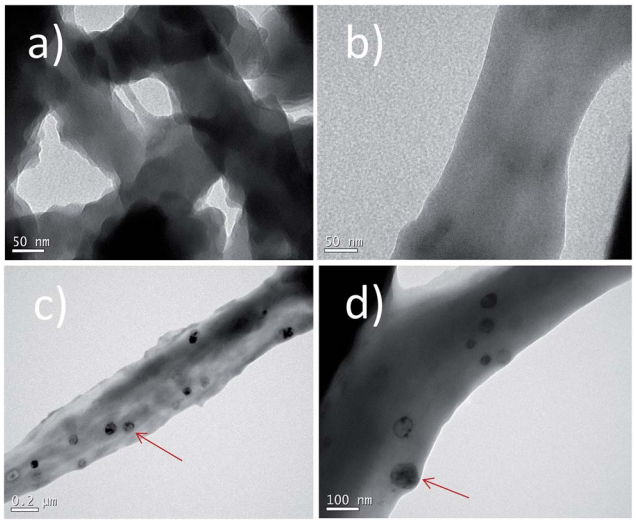

Fig. 5 (a and b) TEM images of pure PANI nanofibers/nanofiber and (c and d) TEM images of PANI–GO samples PG-C at different magnifications. The red arrows point to the stacking of GO nanoplatelets onto the PANI nanofibers.

seen in Fig. 5. A close examination of individual nanofibers morphology indicates the stacking of GO platelets onto the surface of PANI nanofibers (Fig. 5c and d), compared to the pure PANI nanofibers (Fig. 5a and b). The GO platelets with PANI nanofibers are suggesting good compatibility between both components. PANI is a conducting polymer that contains positively charged nitrogen on its polymer chain, which favors the adhesion of GO platelets onto the PANI nanofibers. Hence, it is no wonder that the unique structure of PANI–GO can be considered for high electrochemical performance.

Fig. 6 shows results obtained with AFM and current sensing measurements. The CS-AFM is a powerful technique for characterizing the conductivity of the sample surface. The microscope can apply a constant voltage and monitor the current between the sample and probing tip during the scan. The 3D representation (Fig. 6a) of the topography of bare ITO, pure PANI and PANI–GO samples reveals the rough nature of the electrodeposited surfaces. For bare ITO and pure PANI, a roughness (root mean square fluctuation of height) below 3 nm was measured. The roughness significantly increased with the increase of GO contents in the films, 26 nm for PG-A and 48 nm for PG-C. The rougher surface of PANI–GO films provides a highly accessible surface area for redox activity. In Fig. 6b, the *I–V* curve for bare ITO shows the ohmic behavior while the *I–V* curves for pure PANI and PANI–GO films show typical semiconductor behavior. The differences in the shapes of these *I–V* curves are attributed to the inhomogeneous surface of the films. The current passing through different nanofibers is not same due to the non-uniformity in the height of the nanofibers, as we also can see in SEM results.

The XPS spectrum of the electrodeposited PANI–GO film was obtained to verify the presence of GO and PANI. The XPS spectra of PANI–GO and GO were analyzed, and the comparative results are shown in Fig. 7. The spectrum of PANI–GO (Fig. 7a) with regard to the spectrum of GO (Fig. 7b), shows two new peaks corresponding to the N 1s and S 2p; the peak N 1s comes from PANI and the peak S 2p comes from sulfuric acid, respectively. The presence of S 2p peak in the PANI–GO film indicates that the PANI was also doped by sulfuric acid. As a result, this is a clear signal of the coexistence of both PANI and GO in the electrodeposited film. The core-level spectrum of C 1s for PANI–GO film is shown in ESI (Fig. SI4†), in which the curves fit for various carbon components, *i.e.*, C–C, C–O, C=O, and C–N due to the presence of oxygen and nitrogen species. Signals for C–O and C=O are evidence of GO, and the signal for C–N is evident of PANI. Further evidence in the coexistence of the GO and PANI in the electrodeposited films was provided by the FT-IR spectra as shown in Fig. 8. A typical FT-IR spectrum of GO is shown in Fig. 8a. In agreement with previous work,[38,39] the spectrum shows several bands broadband-centered at 3430 cm^{-1}, attributed to deformation of –OH group. The band at 1740 cm^{-1} is due to carbonyl or carboxylic groups (C=O), the band around 1635 cm^{-1} is due to aromatic C=C, and the band at 1460 cm^{-1} is due to carboxy (C–O), epoxy C–O (1260 cm^{-1}), and alkoxy C–O (1105 cm^{-1}) groups located at the edges and basal planes of GO. The FT-IR spectrum of the electrochemically prepared pure PANI in Fig. 8b shows the bands at 1645 cm^{-1} and 1560 cm^{-1} of the quinonoid and benzenoid units, respectively.[40–42] The bands at 1295 and 1260 cm^{-1} are assigned to the C–N stretching of benzenoid unit, while the band at 1095 cm^{-1} is due to C=N stretching of quinonoid, which are identical to that of the doped PANI, and many low-intensity peaks ranging from 800 to 500 cm^{-1} can be assigned to the vibrations of the C–H bonds in the benzene rings.[43,44] The broad peak in the frequency range of 3445 cm^{-1} is attributed to the N–H stretching vibrations of the emeraldine salt, and the shoulders at 2850–2995 cm^{-1} correspond to aromatic sp^2 C–H stretching.[45] The spectrum (Fig. 8c) of PANI–GO film is showing all characteristic peaks of both PANI and GO. It also observed that the low-intensity peak at

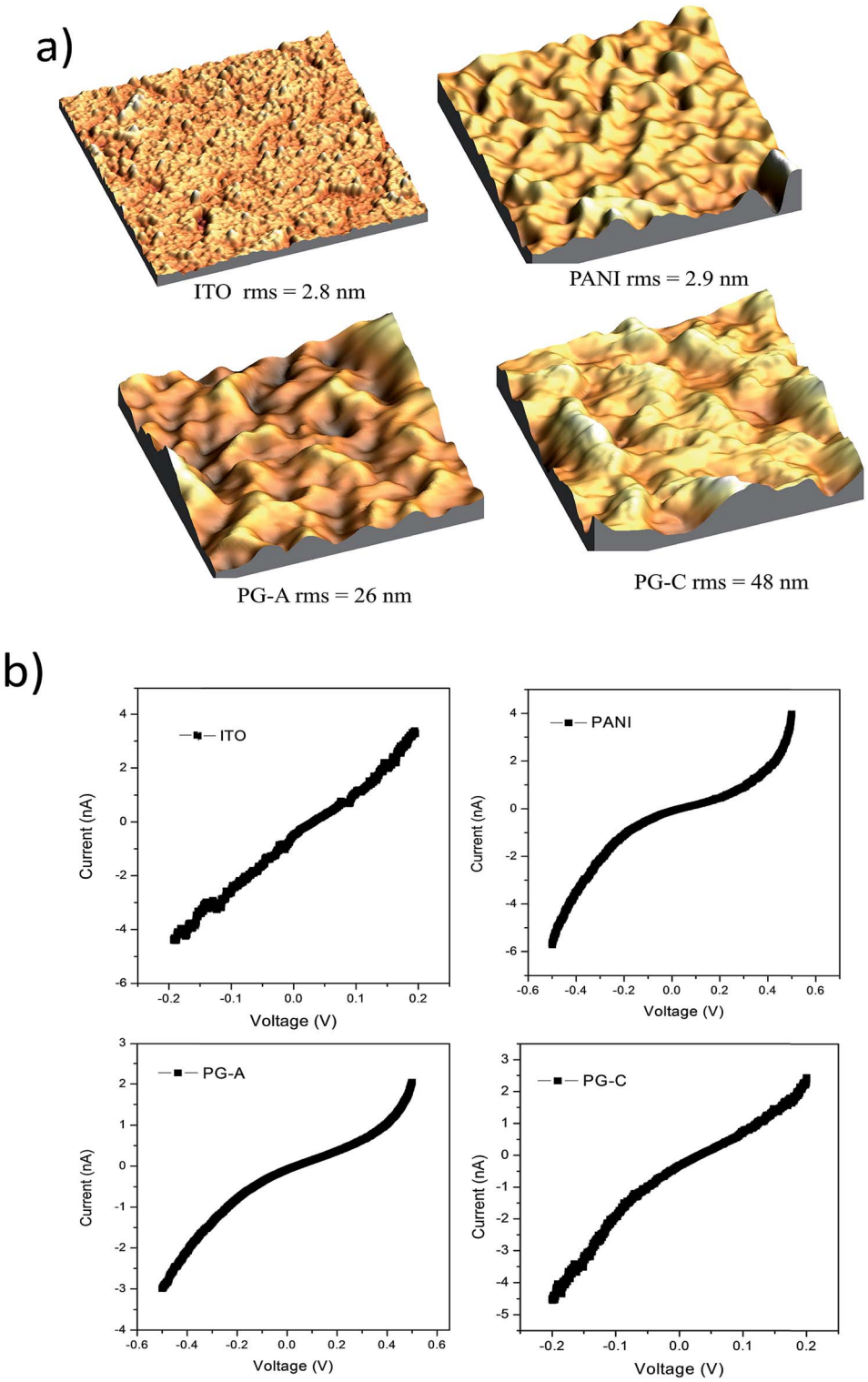

Fig. 6 Topographical 3D AFM images of (a) bare ITO, pure PANI, PG-A, and PG-C, (rms = root mean square of the surface roughness of the films) and (b) *I*–*V* curves of bare ITO, pure PANI, and PANI–GO samples (PG-A, and PG-C).

1299 cm^{-1} in the spectrum of pure PANI becomes more intense in the spectrum of PANI–GO, which is caused by the strong interaction between the amine group of PANI and the oxygenated GO, which clearly supports the adsorption of GO nanoplatelets with PANI nanofibers during the electropolymerization process.

UV-vis spectra of electrodeposited PANI–GO film on the ITO display basically the same absorptive characteristics as that of electrodeposited pure PANI film (H_2SO_4-doped) as shown in

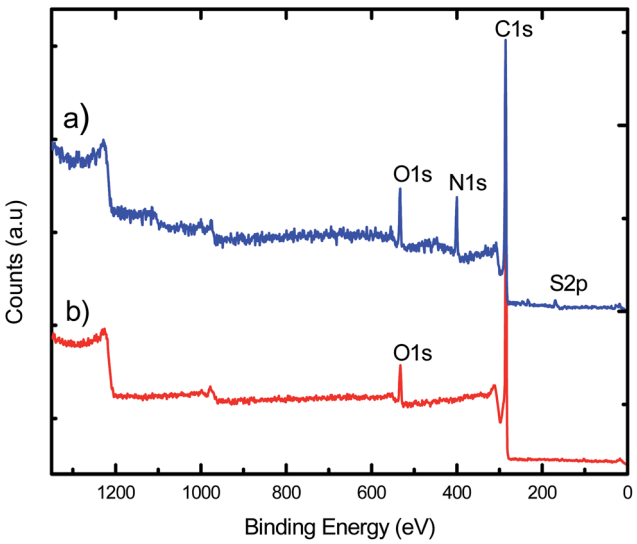

Fig. 7 (a) XPS spectrum of PANI–GO film (PG-C) and (b) XPS spectrum of GO.

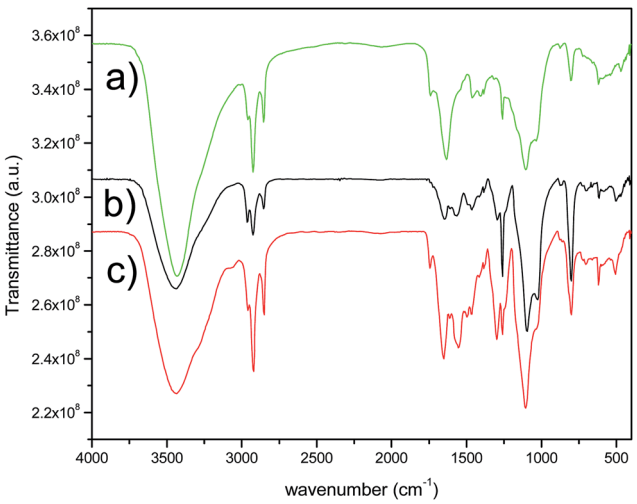

Fig. 8 FTIR spectra of (a) GO, (b) pure PANI, and (c) PANI–GO (PG-C).

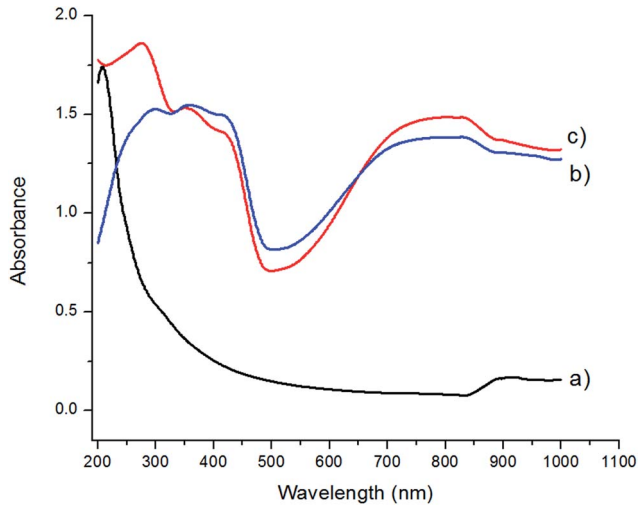

Fig. 9 UV-vis spectra of (a) GO, (b) pure PANI nanofibers (H_2SO_4-doped), and (c) PANI–GO (PG-C).

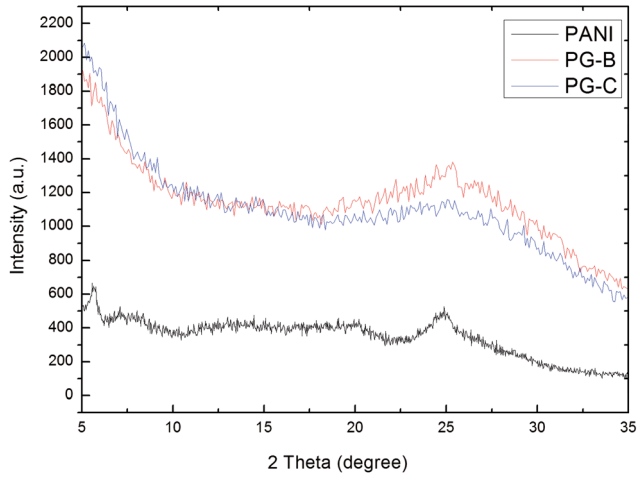

Fig. 10 XRD patterns of pure PANI and PANI–GO.

Fig. 9b and c. The peaks at ~300 and 800 nm are attributed to the benzenoid and quinoid rings, respectively.[46,47] Additionally, after the adsorption of GO nanoplatelets onto PANI nanofibers, the peak at 284 nm of the PANI–GO film blue shifts by 15 nm, compared with the pure PANI film, indicating the interaction of GO with PANI. The absorption peak of the GO could be observed at 215 nm (Fig. 9a). The structure of the PANI–GO film was also examined by powder XRD measurements. The XRD patterns of pure PANI and PANI–GO samples (PG-B, and PG-C) are shown in Fig. 10. The pure PANI exhibits several broad reflection peaks with the most intense peaks centered at $2\theta = 25°$, and the peak at $2\theta = 5.9°$ can be ascribed to the orientation of the acids (H_2SO_4) in the polyaniline chain.[40–50] Upon the anchoring of GO nanoplatelets onto the PANI nanofibers, the peaks have widened in comparison with the pattern of pure PANI nanofibers, which have been believed to be the reflection of GO nanoplatelets. Therefore, the XRD result verifies the presence of GO into the electrodeposited PANI–GO film.

3.2 Electrochemical performance of PANI–GO thin film electrodes

All electrochemical measurements were based on a three-electrode cell system. A platinum sheet was used as the counter electrode, an SCE electrode was used as a reference electrode and the thin films of PANI–GO and pure PANI on the ITO substrate were used as working electrodes. The electrolyte (1 mol L^{-1} H_2SO_4) was used for all electrochemical tests. Fig. 11 a illustrates the CV curves of samples PG-A, PG-B, PG-C, and pure PANI at a scan rate of 10 mV s^{-1} in the potential window of −0.2 to 0.8 V. From the figure, the remarkable difference of electrochemical surface activity between pure PANI and PANI–GO films can be easily recognized. The redox current peak of pure PANI film is much lower compared to PANI–GO films at the

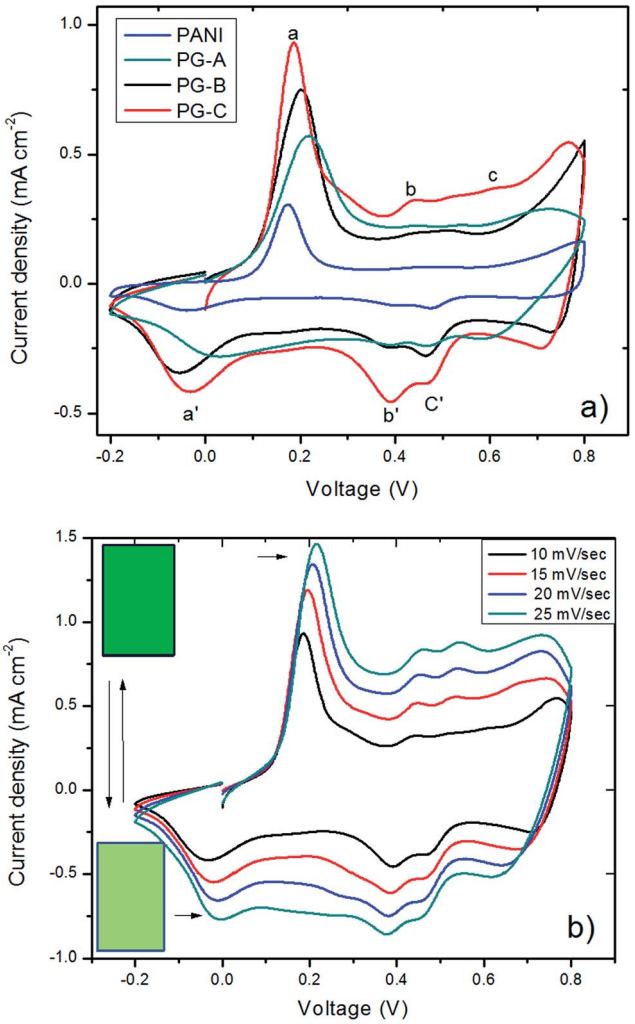

Fig. 11 (a) CV curves of PANI and PANI–GO films at a scan rate of 10 mV s^{-1} in 1 mol L^{-1} H_2SO_4 aqueous solution, and (b) CV curves of PG-C at different scan rates (note: the schematic diagram in (b) the dark and light-green color boxes representing the electrochromatic behavior of PANI–GO film).

same scan rate of 10 mV s^{-1}. It is commonly believed that the electrochemical capacitance is proportional to the area under the CV curve; the area under the CV curves of PANI–GO films is much larger than that of pure PANI film. This indicates a typical pseudocapacitance behavior of PANI–GO films, caused by a redox reaction at the electrode. The PANI undergoes intrinsic redox process electrochemically. The CV curves of PANI–GO films demonstrate the three couples of redox peaks (aa′, bb′ and cc′) in the range of −0.1 to +0.7 V, where the redox pair aa′ correspond to the reversible transition between the leucoemeraldine (reduced form of PANI) and emeraldine forms of PANI (half-oxidized form of PANI).[51] The redox pair cc′ is ascribed to reversible transition between emeraldine and pernigraniline (fully oxidized form of PANI).[52] The middle pair bb′ either is the transition between benzoquinone/aminoquinone couple of PANI[53] or may be due to the transition between quinone/hydroquinone groups of GO.[54]

Herein, it can be speculated that the introduction of GO induced the synergistic effect between PANI nanofibers and GO nanoplatelets, as well as improving the electrode/electrolyte contact surface area for electronic or electrolyte ion transport, which is valuable for enhancing the use of active materials.[29,51] Such electrochemical properties indicate that in this investigation, PG-C is the most promising material for use in supercapacitor thin film electrode of this type. To further investigate the influence of the scan rates, we measured the rate-dependent cyclic voltammograms of PANI–GO (PG-C) electrodes ranging from 10 to 25 mV s^{-1}. It can be found from Fig. 11b that the PANI–GO films exhibit similar curves as the scan rate increased from 10 to 25 mV s^{-1}, indicating good rate capability for the PANI–GO electrode film. It is also important to note that the cathodic peak shifted positively with an increase in the sweep rates from 10 to 25 mV s^{-1}. The positive shifting of the cathodic peak is mainly due to a slight increase in the resistance of the electrolyte at high sweep rates. We also observed the electrochromic behavior of the films during the CV experiment; PANI–GO films exhibited changes in color (dark green to light green and *vice versa*, as shown by schematic diagram in Fig. 11b).

The specific capacitance values were assessed by galvanostatic charge–discharge cycling measurements. This method is more reliable for characterizing the capacitance of the materials under controlled current conditions. The capacitance values of the samples were estimated according to the following equation: specific capacitance (F g^{-1}) = $I/(m\mathrm{d}V/\mathrm{d}t)$, where I is the discharge current in amperes, m is the mass (gram) of active material on the substrate, and dt is the discharge time (s) corresponding to the voltage difference dV in volts. dV/dt can be obtained from the slope of the discharge curve. The galvanostatic charge–discharge cycles were examined at various current densities from 0.025 to 0.25 mA cm^{-2}. The curve of PANI–GO films in Fig. 12 a show longer charge–discharge duration than pure PANI film, which means that it possesses higher specific capacitance than pure PANI. A high specific capacitance value of 662 F g^{-1} was obtained for sample PG-C at a constant low-current density of 0.025 mA cm^{-2}, whereas the pure PANI film has minimal capacitance of 256 F g^{-1} at the same current density. Thus, the greatly increased specific capacitance can be ascribed from the synergistic contribution of PANI nanofibers and GO nanoplatelets combined with the merits of the interconnected nanofiber porous structure of the film. In other words, both components cannot offer high specific capacitance individually but together provide an enhanced electrode/electrolyte interface area accessible for redox reaction during charge–discharge processes, making them fully electrochemically accessible. Therefore, the electrochemical property of the PANI–GO was improved effectively. The variation of the specific capacitance with the current density is shown in Fig. 12b, which shows that the specific capacitance decreases significantly with the increment of scan-current density and can be achieved as high as 580 F g^{-1}, even at a 10 times higher discharge current density of 0.25 mA cm^{-2}. This marks the good rate capability of the PANI–GO film (PG-C), which is recognized as one of the most important electrochemical properties in the application of thin film electrode materials.

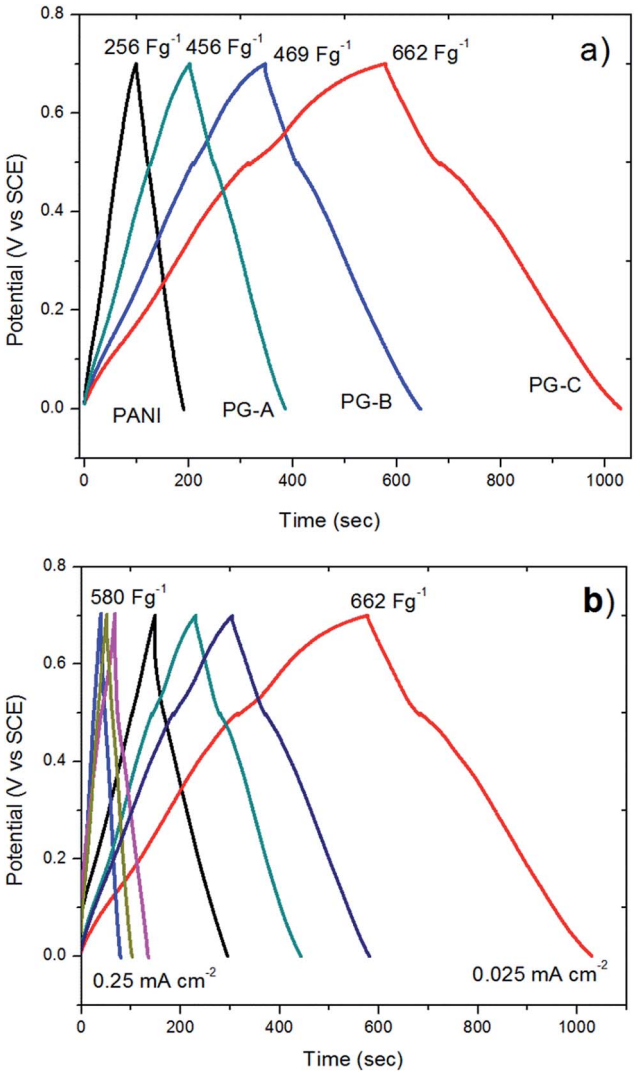

Fig. 12 (a) Galvanostatic charge–discharge curves of pure PANI and PANI–GO thin film electrodes at a current density of 0.025 mA cm^{-2} within a potential window of 0–0.7 V in 1 mol L^{-1} H_2SO_4 and (b) charge–discharge curves of PG-C thin film electrode at different current densities in 1 mol L^{-1} H_2SO_4.

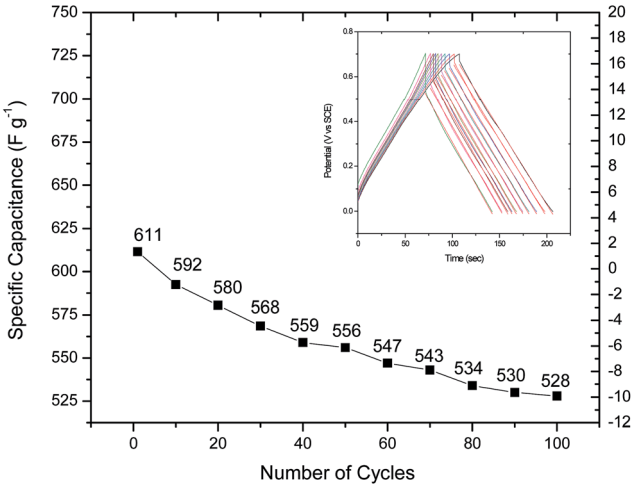

Fig. 13 Charge–discharge cyclic performance of PG-C thin film electrode at a current density of 0.1 mA cm^{-2} in 1 mol L^{-1} H_2SO_4 (inset: charge–discharge curves of 100 cycles, each one contains 10 cycles).

Thus, we believe that in our system, the high capacitance of electrodeposited PANI–GO films is anticipated due to the unique microstructure of materials, which provide the ideal synergistic interaction between PANI nanofibers and GO nanoplatelets. The electrochemical stability of PG-C film was examined under continuous charge–discharge tests at 0.1 mA cm^{-2} for 100 cycles. As shown in Fig. 13, there is a small decrease in the specific capacitance value of sample PG-C in the 100 cycles, and thereafter, the specific capacitance remains almost constant. The decrease in the specific capacitance was 10% in the 100 cycles. The instability of the capacitors based on electrochemically prepared films during a long-term charge–discharge cycling experiment is one of the most serious problems. Our films could not be reused after a prolonged experiment because the electrodeposited film of PANI–GO started to peel off from the ITO surface. To overcome this drawback, work is under way in our lab for the construction of longer-lasting thin film electrodes with high specific capacitance. Energy density and power density are also used as important factors for supercapacitors. Specific energy and specific power have been derived from galvanostatic charge–discharge at various current densities using the following equations: specific energy (W h kg^{-1}) = $[ItV]/m$ and specific power (W kg^{-1}) = $[IV]/m$, in which discharge current (I), time (t) spent in discharge, mass (m), and voltage (V) are in amperes, seconds, kilograms, and volts, respectively. The evaluated values of specific energy and specific power are shown in Fig. 14. At a specific energy of 64.5 W h kg^{-1}, specific power of 1159 W kg^{-1} was obtained at the current scan rate of 1.6 A g^{-1}. Specific power as high as 17 500 W kg^{-1} was obtained with the specific energy of 34 W h kg^{-1} at the current scan rate of 25 A g^{-1}. These values are comparable with the earlier reported results for thin film electrode materials in the three-electrode cell system.[55,56]

Electrical characterization was performed for all samples in 1 mol L^{-1} H_2SO_4 aqueous electrolyte by electrochemical impedance spectroscopy (EIS). This is a useful technique to analyze the frequency-dependent electrochemical response of the system. The EIS data have been analyzed by using Nyquist plots. This plot shows the frequency response of the electrode/electrolyte system and is a plot of the imaginary component (Im $\{Z\}$) of the impedance against the real component (Re$\{Z\}$). Fig. 15 displays a Nyquist plot for PANI and PANI–GO samples, the semicircle for the high-frequency region and the vertical–linear characteristic in the mid-to-low frequency regions were observed. The circuit parameters, such as series impedance, charge-transport impedance, and characteristic frequencies were extracted by fitting the semicircles, assuming that the system response follows a modified Randles circuit. We observed that the double-layer charge transport has a characteristic frequency of 2.4 kHz for pure PANI film and 370 Hz for PANI–GO films. The electrical resistivities calculated using charge–transport resistance values at 0 V were 1.5 MΩ cm for

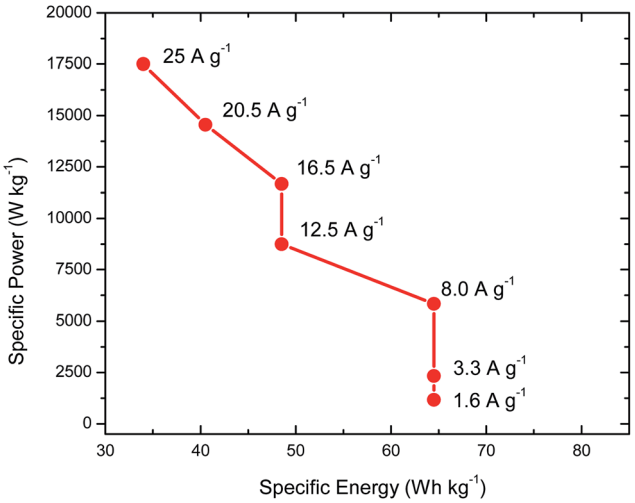

Fig. 14 Ragone plot of specific energy *vs.* specific power at different specific currents.

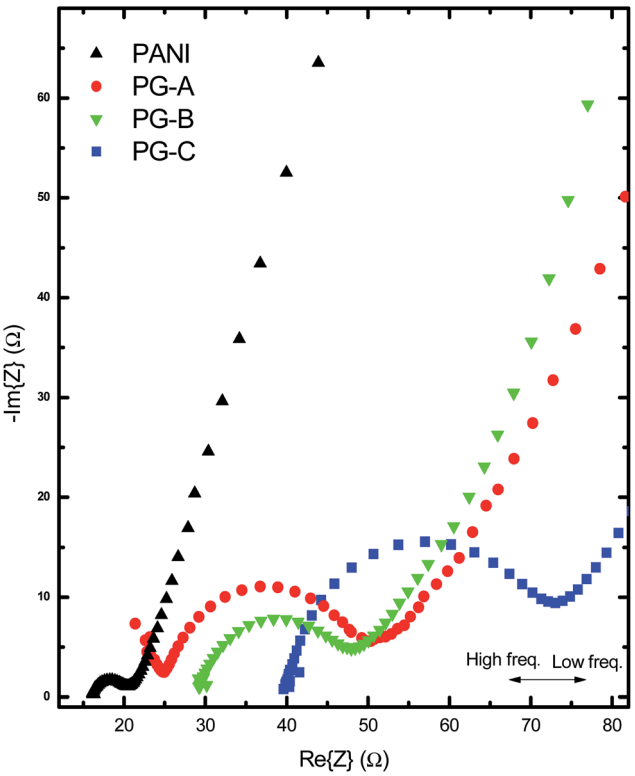

Fig. 15 Nyquist plots for pure PANI and PANI–GO (▲ PANI, ● PG-A, ▼ PG-B, ■ PG-C).

pure PANI and between 5 to 9 MΩ cm for PANI–GO samples. The electrolyte resistance was only observed for PANI samples of about 16 Ω, due to frequency limitations. The resistance increased with an increase in the amount of GO in the electrolyte mixture due to the nonconductive nature of GO. Here, it is in contrast with Zhang's reported work,[57] and he found that when composited with PANI, GO demonstrates higher conductivity at lower concentrations due to the increase of the doping degree of PANI. Because the charge-transport resistance remains almost constant, the lower frequencies observed for PANI–GO samples could be attributed to an increase in the capacitance of the samples.

4. Conclusions

In conclusion, composite thin films of graphene oxide nanoplatelets and polyaniline nanofibers have been successfully co-deposited by using a simple one-step electrochemical method. The resulting films have a dense, interconnected nanofiber structure and appear to consist of GO nanoplatelets in SEM and TEM images. Thus, obtained PANI–GO films exhibited excellent electrochemical properties. The greatly enhanced electrochemical performances of PANI–GO thin film electrodes are due to the synergistic combination between the PANI nanofibers and GO nanoplatelets. The specific energy of the thin film electrode material is evaluated at several specific power values, and the Ragone diagram is plotted. Further optimization may be possible by fine-tuning the synthetic conditions. The approach described here may be applicable to other conducting polymers with GO nanoplatelets. Such thin film electrode materials are inevitably required for thin film microbatteries and ultracapacitors.

Acknowledgements

Author M.K. would like to place in record his special thanks to the CAPES/PNPD, Government of Brazil for providing post-doctoral fellowship to carry out part of the research work in the physics department of UFSC, Florianopolis. The authors also thank to Prof. A. Neves (LBC/UFSC, Brazil) for providing FTIR facilities and other Brazilian funding agencies, including FINEP, CNPq and FAPESC.

References

1 P. Simon and Y. Gogotsi, *Nat. Mater.*, 2008, **7**, 845–854.
2 M. Jayalakshmi and K. Balasubamanyam, *Int. J. Electrochem. Sci.*, 2008, **3**, 1196–1217.
3 C. Yuan, B. Gao, L. Shen, S. Yang, L. Hao, J. X. Lu, F. Zhang, J. L. Zhang and G. X. Zhang, *Nanoscale*, 2011, **3**, 529–545.
4 S. W. Lee, B. M. Gallant, H. R. Byon, P. T. Hammond and Y. Shao-Horn, *Energy Environ. Sci.*, 2011, **4**, 1972–1985.
5 M. Liu, Y. E. Miao, C. Zhang, W. W. Tjiu, Z. Yang, H. Peng and T. Liu, *Nanoscale*, 2013, **5**, 7312–7320.
6 K. R. Prasad and N. Munichandraiah, *J. Power Sources*, 2002, **112**, 443–451.
7 M. Mecklenburg, A. Schuchardt, Y. K. Mishra, S. Kaps, R. Adelung, A. Lotnyk, L. Kienle and K. Schulte, *Adv. Mater.*, 2012, **24**, 3486–3490.
8 X. B. Yan, Z. X. Tai, J. T. Chen and Q. J. Xue, *Nanoscale*, 2011, **3**, 212–316.
9 S. X. Xiong, F. Yang, H. Jiang, J. Ma and X. H. Lu, *Electrochim. Acta*, 2012, **85**, 235–242.

10 X. J. Lu, H. Dou, S. D. Yang, L. Hao, L. J. Zhang, L. F. Shen, F. Zhang and X. G. Zhang, *Electrochim. Acta*, 2011, **56**, 9224–9232.
11 F. Kim, L. J. Cote and J. Huang, *Adv. Mater.*, 2010, **22**, 1954–1958.
12 H. He, J. Klinowski, M. Forster and A. Lerf, *Chem. Phys. Lett.*, 1998, **287**, 53–56.
13 A. Lerf, H. He, M. Forster and J. Klinowski, *J. Phys. Chem. B*, 1998, **102**, 4477–4482.
14 G. Wang, W. Xing and S. Zhuo, *Electrochim. Acta*, 2012, **66**, 151–157.
15 K. Zhang, L. L. Zhang, X. S. Zhao and J. Wu, *Chem. Mater.*, 2010, **22**, 1392–1401.
16 E. Coskun, E. A. Z-Contreras and H. J. Salavagione, *Carbon*, 2012, **50**, 2235–2243.
17 Z. Cui, C. X. Guo, W. Yuan and C. M. Li, *Phys. Chem. Chem. Phys.*, 2012, **14**, 12823–12828.
18 A. K. Mishra and S. Ramaprabhu, *J. Mater. Chem.*, 2012, **22**, 3708–3712.
19 H. L. Wang, Q. L. Hao, X. J. Yang, L. D. Lu and X. Wang, *ACS Appl. Mater. Interfaces*, 2010, **2**, 821–828.
20 B. Xu, S. F. Yue, Z. Y. Sui, X. T. Zhang, S. S. Hou, G. P. Cao and Y. S. Yang, *Energy Environ. Sci.*, 2011, **4**, 2826–2830.
21 S. Liu, X. H. Liu, Z. P. Li, S. R. Yang and J. Q. Wang, *New J. Chem.*, 2011, **35**, 369–374.
22 Q. Wu, Y. X. Xu, Z. Y. Yao, A. R. Liu and G. Q. Shi, *ACS Nano*, 2010, **4**, 1963–1970.
23 Y. Li, H. Peng, G. Li and K. Chen, *Eur. Polym. J.*, 2012, **48**, 1406–1412.
24 J. Li, H. Xie, Y. Li, J. Liu and Z. Li, *J. Power Sources*, 2011, **196**, 10775–10781.
25 H. Gomez, M. K. Ram, F. Alvi, P. Villalba, E. Stefanakos and A. Kumar, *J. Power Sources*, 2011, **196**, 4102–4108.
26 F. Chen, P. Liu and Q. Zhao, *Electrochim. Acta*, 2012, **76**, 62–68.
27 G. Wang, S. Zhuo and W. Xing, *Mater. Lett.*, 2012, **69**, 27–29.
28 W. L. Zhang, Y. D. Liu and H. J. Choi, *Carbon*, 2012, **50**, 290–296.
29 J. J. Xu, K. Wang, S. Z. Zu, B. H. Han and Z. X. Wei, *ACS Nano*, 2010, **4**, 5019–5026.
30 Q. Zhang, Y. Li, Y. Feng and W. Feng, *Electrochim. Acta*, 2013, **90**, 95–100.
31 X. M. Feng, R. M. Li, Y. W. Ma, R. F. Chen, N. E. Shi, Q. L. Fan and W. Huang, *Adv. Funct. Mater.*, 2011, **21**, 2989–2996.
32 D. W. Wang, F. Li, J. P. Zhao, W. C. Ren, Z. G. Chen, J. Tan, Z. S. Wu, L. Gentle, G. Q. Lu and H. M. Cheng, *ACS Nano*, 2009, **3**, 1745–1752.
33 J. Yan, T. Wei, B. Shao, Z. J. Fan, W. Z. Qian, M. L. Zhang and F. Wei, *Carbon*, 2010, **48**, 487–493.
34 A. Dimiev, D. V. Kosynkin, L. B. Alemany, P. Chaguine and J. M. Tour, *J. Am. Chem. Soc.*, 2012, **134**, 2815–2822.
35 W. S. Hummers and R. E. Offeman, *J. Am. Chem. Soc.*, 1958, **80**, 1339.
36 L. J. Cote, F. Kim and J. Huang, *J. Am. Chem. Soc.*, 2009, **131**, 1043–1049.
37 H. Randriamahazaka, V. Noel and C. Chevrot, *J. Electroanal. Chem.*, 1999, **472**, 103–111.
38 X. Huang, N. Hu, R. Gao, Y. Yu, Y. Wang, Z. Yang, E. S.-W. Kong, H. Weia and Y. Zhang, *J. Mater. Chem.*, 2012, **22**, 22488–22495.
39 Y. Zhao, G.-S. Tang, Z.-Z. Yu and J.-S. Qi, *Carbon*, 2012, **50**, 3064–3073.
40 Z. Ping, H. Neugebauer and A. Neckel, *Electrochim. Acta*, 1996, **41**, 767–772.
41 Z. Ping, G. E. Nauer, H. Neugebauer, J. Theiner and A. Neckel, *J. Chem. Soc., Faraday Trans.*, 1997, **93**, 121–129.
42 A. Kellenberger, E. Dmitrieva and L. Dunsch, *J. Phys. Chem. B*, 2012, **116**, 4377–4385.
43 Y. Li, X. Zhao, Q. Xu, Q. Zhang and D. Chen, *Langmuir*, 2011, **27**, 6458–6463.
44 H. Gu, Y. Huang, X. Zhang, Q. Wang, J. Zhu, L. Shao, N. Haldolaarachchige, D. P. Young, S. Wei and Z. Guo, *Polymer*, 2011, **53**, 801–809.
45 X. B. Yan, Z. J. Han, Y. Yang and B. K. Tay, *Sens. Actuators, B*, 2007, **123**, 107–113.
46 J. X. Huang, S. Virji, B. H. Weiller and R. B. Kaner, *J. Am. Chem. Soc.*, 2003, **125**, 314–315.
47 J. X. Huang and R. B. Kaner, *J. Am. Chem. Soc.*, 2004, **126**, 851–855.
48 Z. M. Zhang, M. X. Wan and Y. Wei, *Adv. Funct. Mater.*, 2006, **16**, 1100–1104.
49 T. Jana, J. Chatterjee and A. K. Nandi, *Langmuir*, 2002, **18**, 5720–5727.
50 Z. D. Zujovic, C. Laslau, G. A. Bowmaker, P. A. Kilmartin, A. L. Webber, S. P. Brown and J. Travas-Sejdic, *Macromolecules*, 2010, **43**, 662–670.
51 Y. G. Wang, H. Q. Li and Y. Y. Xia, *Adv. Mater.*, 2006, **18**, 2619–2623.
52 C. C. Hu and C. H. Chu, *Mater. Chem. Phys.*, 2000, **65**, 329–338.
53 Y. H. Lee, C. Z. Chang, S. L. Yau, L. J. Fan and Y. W. Yang, *J. Am. Chem. Soc.*, 2009, **131**, 6468–6474.
54 Y. R. Nian and H. S. Teng, *J. Electrochem. Soc.*, 2002, **149**, 1008–1014.
55 Md. M. Sk, C. Y. Yue and R. K. Jena, *Polymer*, 2014, **55**, 798–805.
56 V. Gupta and N. Miura, *Electrochem. Solid-State Lett.*, 2005, **8**, A630–A632.
57 K. Zhang, L. L. Zhang, X. S. Zhao and J. S. Wu, *Chem. Mater.*, 2010, **22**, 1392–1401.

